



Article

Enhancement of the Ionic Conductivity in Electric Field-Assisted Pressureless Sintered BITIVOX Solid Electrolytes

Midilane S. Medina¹, Sabrina G. M. Carvalho¹ , Eliana N. S. Muccillo¹  and Reginaldo Muccillo^{1,2,*}

¹ Center of Science and Technology of Materials—CCTM, Energy and Nuclear Research Institute—IPEN, S. Paulo, SP 05508-170, Brazil

² Center of Engineering, Modeling and Applied Social Sciences, Federal University of ABC, Santo André, SP 09210-580, Brazil

* Correspondence: muccillo@usp.br; Tel.: +55-11-3133-9203

Received: 16 June 2019; Accepted: 25 July 2019; Published: 11 August 2019



Abstract: $\text{Bi}_4\text{V}_{1.8}\text{Ti}_{0.2}\text{O}_{11}$ (BITIVOX) ceramic pellets, prepared with powders obtained by a sol gel technique, were sintered either conventionally at 800 °C/8 h or by applying an AC electric voltage, limiting the electric current through the pellets. Electric voltages were applied isothermally at 700 °C and 800 °C during 5 min in the green pellet positioned in the sample holder of a dilatometer for monitoring thickness variation. The BITIVOX pellets shrank 13.6% after applying 200 V cm^{-1} at 800 °C and 10.4% heating to 800 °C for 8 h. Thermal analysis and X-ray diffraction of the powders were performed to evaluate the crystallization temperature and the structural phase, respectively. The electrical behavior of the sintered BITIVOX pellets was analyzed by the impedance spectroscopy technique, showing that the sample flash sintered at 800 °C/5 min had lower bulk resistivity than the sample conventionally sintered at 800 °C/8 h. The surfaces of the sintered pellets were observed in a scanning electron microscope showing similar grain sizes and pore content in all sintered samples.

Keywords: BIMEVOX; solid electrolyte; flash sintering; impedance spectroscopy

1. Introduction

Oxide ion ceramic solid electrolytes find uses in many commercial devices, e.g., solid oxide fuel cells (SOFCs), oxygen sensors, and oxygen electrochemical pumps [1–6]. The most important ceramic solid electrolyte is the cubic fully stabilized zirconia ZrO_2 : 8 mol% Y_2O_3 (8YSZ), which is a component of SOFCs with 0.01 S cm^{-1} electrical conductivity at 800 °C to ensure high power densities [7]. Since 1982 solid electrolytes with oxide ion conductivity higher than that of 8YSZ have been proposed: CeO_2 :20 mol% Gd_2O_3 (GDC, gadolinia-doped ceria) in 1982 [8], $\text{Bi}_4\text{V}_{2-x}\text{Me}_x\text{O}_{11}$ (BIMEVOX) in 1990 [9], CeO_2 :20 mol% Sm_2O_3 (SDC, samaria-doped ceria) in 1992 [10], $\text{La}_{0.9}\text{Sr}_{0.1}\text{Ga}_{0.8}\text{Mg}_{0.2}\text{O}_{3-\delta}$ (LSGM, strontium- and magnesium-doped lanthanum gallate) in 1996 [11], and $\text{La}_2\text{Mo}_2\text{O}_9$ (LAMOXY, lanthanum molybdenum oxide) in 2000 [12]. A solid electrolyte with ionic conductivity higher than that of 8YSZ would allow for designing SOFCs operating at lower temperatures, thus reducing misfit problems between solid electrolyte and other components in those devices, like anode and cathode.

BIMEVOX solid electrolytes are obtained by partially replacing V^{5+} with pentavalent or aliovalent ions in the $\text{Bi}_4\text{V}_2\text{O}_{11}$ compound. Several BIMEVOX compounds have been synthesized with single or double replacements with several different metallic ions, Li^+ , Cu^{2+} , Co^{2+} , Ni^{2+} , Zn^{2+} , Fe^{3+} , Al^{3+} , Ti^{4+} , Zr^{4+} , Ge^{4+} , Sn^{4+} , Pb^{4+} , Nb^{5+} [13–32]. The structural phases of $\text{Bi}_4\text{V}_2\text{O}_{11}$ are monoclinic (named alpha), orthorhombic from 445 °C (beta) and tetragonal from 567 °C (gamma), the gamma phase

with the highest oxygen ion conductivity [23,32]. The tetragonal gamma phase may be partially or fully stabilized at room temperature by aliovalent replacements for V^{5+} . Therefore, bismuth oxide and doped bismuth oxide systems exhibit a complex set of crystallographic structures and electrical properties, which depend upon temperature, atmosphere, dopant type, and concentration. The best bismuth-based ionic conductor is the $Bi_4V_{1.8}Ti_{0.2}O_{10.9}$ compound.

Flash sintering (FS) is an electric field-assisted pressureless sintering technique accomplished in short times, from seconds to minutes, in comparison with the time required in conventional sintering (hours). That technique has been widely applied to sinter several electroceramics at temperatures lower than those used in conventional sintering, producing consolidated bodies without considerable grain growth [33–38]. Sintering to near full density with that technique may be achieved by applying moderate electric fields (tens of Volts) with limiting currents (mA to few A range) to green ceramic pellets isothermally at temperatures below the conventional temperature for sintering, saving time and energy consumption.

The synthesis by the complex polymerization chemical method of BITIVOX powders and the conformation by electric field-assisted (flash) pressureless sintering at temperatures similar to and lower than those previously conventionally used for sintering (700 °C and 800 °C) are here reported for the first time. Microstructural analysis and impedance spectroscopy measurements show the possibilities of electric field-assisted pressureless sintering BITIVOX ceramic ionic conductors with improved electrical behavior.

2. Materials and Methods

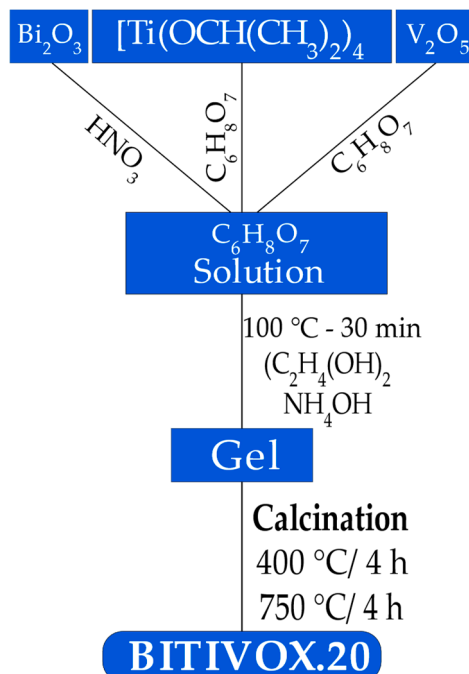
Polycrystalline $Bi_4V_{1.8}Ti_{0.2}O_{11}$ powders were synthesized by the complex polymerization method with bismuth trioxide (Bi_2O_3 , Riedel-de-Haen), vanadium pentoxide (V_2O_5 , Alfa Aesar 99.2%), titanium (IV) isopropoxide [$Ti(OCH(CH_3)_2)_4$, Sigma Aldrich 99.999%], citric acid ($C_6H_8O_7$, CAAL) and ethane-1,2-diol ($C_2H_4(OH)_2$, ethylene glycol, Vetec, Sigma-Aldrich, St. Louis, MI, USA) according to the Schema shown below. To prepare a solution with titanium, stoichiometric amounts of Bi_2O_3 were dissolved in nitric acid (HNO_3 , Vetec, Sigma-Aldrich, St. Louis, MI, USA), V_2O_5 in citric acid, and [$Ti(OCH(CH_3)_2)_4$] was dropwise dissolved in citric acid. The TiO_2 content was evaluated by gravimetric analysis. The citric acid/metal molar ratio was kept at 4:1. The solution was mixed and stirred at ~100 °C until it turned homogeneous; ammonium hydroxide (NH_4OH , Synth) was used to adjust the pH to 7. Afterwards, ethylene glycol was added to promote the citrate polymerization, fixing at 60:40 the mass ratio of the citric acid/ethylene glycol. The solution was then kept under magnetic stirring for several hours up to obtaining a gel. The gel was analyzed by simultaneous thermogravimetric (TG) and differential thermal analysis (DTA) from room temperature to 1000 °C at 10 °C min^{-1} rate under flowing synthetic air in a simultaneous thermal analyzer (Netzsch STA 409E, Selb, Germany).

The powder, after calcination at 750 °C for removing organics, was pressed uniaxially (50 MPa) into $\varnothing 5.0 \times 2.5$ mm pellets and isostatically (200 MPa).

X-ray diffraction analyses were carried out in the synthesized ceramic powders and in ground powders of sintered BITIVOX pellets in a diffractometer (D8 Advance, Bruker-AXS, Karlsruhe, Germany) in Bragg-Brentano configuration with $Cu-k_\alpha$ radiation, scintillation detector, in the 25–60° 2θ range, 0.05° step size, 5 s per step.

For the flash sintering experiments, BITIVOX cylindrical pellets were positioned into the sample holder of a vertical dilatometer (Unitherm 1161, Anter, Pittsburgh, PA, USA). Platinum grids, placed on both parallel surfaces of the sample, were connected with platinum wires to a custom-made power supply operating at 50–60 V, 1.0 A, 1.1 kHz. The applied voltage and the electric current through the specimen were collected with two Fluke 8050 A multimeters and stored in a computer [39]. The experimental procedure for flash sintering consisted on applying an electric voltage during 5 min when the temperature of the specimen reached 700 °C or 800 °C, monitoring voltage and current pulses with the multimeters, and specimen thickness shrinkage ($\pm 1 \mu m$) with the dilatometer gauge. Typical

electric field and current profiles are shown in Figure 1, with initial field and current peaks, the voltage decreasing to a value dependent on the electrical resistance of the sample, to keep constant the pre-set current. The inset shows that the incubation time, i.e., the elapsed time to the occurrence of the electric current pulse, is 3.2 s and the half-width of the electric current pulse is approximately 0.5 s.



Schema. Experimental sequence for the synthesis of $\text{Bi}_4\text{V}_{1.8}\text{Ti}_{0.2}\text{O}_{11}$ (BITIVOX) ceramic powders.

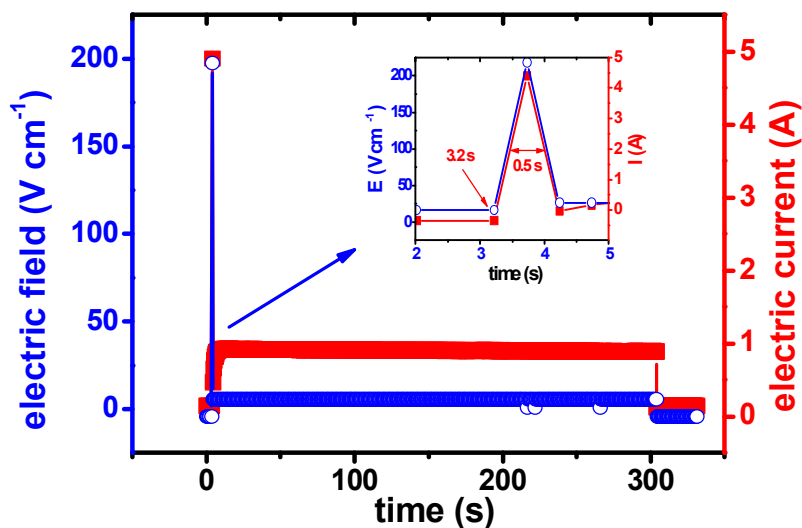


Figure 1. Time evolution of applied electric field and electric current through a BITIVOX pellet during 300 s at 800 °C. Inset: exploded view of the first 5 s under the electric field.

The apparent hydrostatic density of the sintered samples was evaluated by the Archimedes method in a Mettler Toledo AG245 analytical balance (Columbus, OH, USA) with a special density determination kit. The evaluated values were in the 76%–83% T.D. range (T.D.: theoretical density, 7.74 g cm⁻³ apud [31]): 5.86 g cm⁻³ (76.2% T.D.), 6.00 g cm⁻³ (77.5) and 6.43 g cm⁻³ (83.1) for the specimens flash sintered at 700 °C, heat-treated at 800 °C/8 h and flash sintered at 800 °C, respectively. Denser specimens could be obtained by stripping the external surfaces of the flash sintered specimen.

Impedance spectroscopy measurements were carried out with a Hewlett Packard 4192 A impedance analyzer (Yokogawa-Hewlett Packard, Tokyo, Japan) in the 275 °C–400 °C temperature range from 5 Hz to 13 MHz, 16 points per decade, with 200 mV input AC voltage. Three cylindrical samples, with their parallel surfaces covered with silver electrodes, were spring-loaded in a sample chamber with platinum disk electrodes and leads, which was positioned inside a programmable furnace. $[-Z''(\omega) \times Z'(\omega)]$ impedance data were collected with a special software [40].

Scanning electron microscopy images were observed with a FEG-SEM microscope (Inspect F50, FEI, Brno, Czech Republic) in the flat surfaces of the sintered pellets.

3. Results and Discussion

The thermogravimetric and differential thermal analyses of the synthesized BITIVOX gel are shown in Figure 2. These curves exhibit two main thermal events: a weight loss due to dehydration and evaporation of volatiles, besides the decomposition of free citric acid (added in excess during synthesis) and initial decomposition of the organic matter from room temperature to approximately 200 °C and an exothermic peak related to organic decomposition from 200 °C to approximately 480 °C. The inflection of the peak close to 550 °C points out to the beginning of the crystallization process. Based on these results, calcination at 750 °C was then carried out for producing the BITIVOX powders.

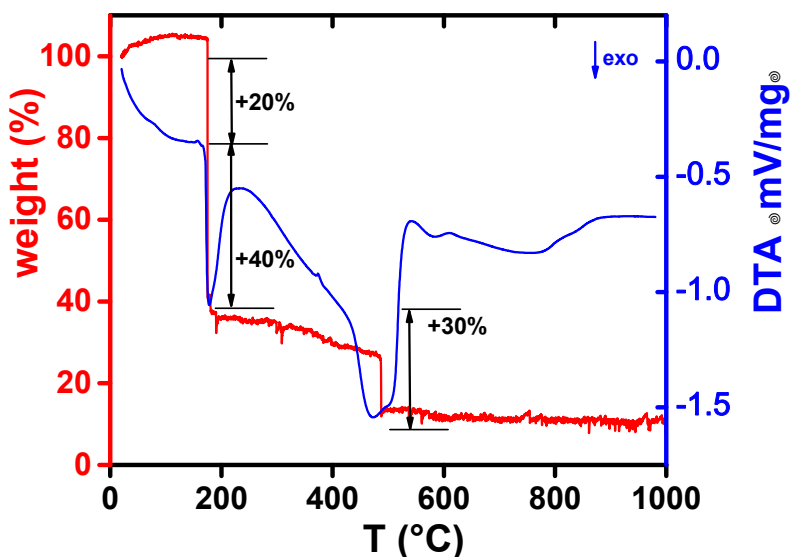


Figure 2. Thermogravimetric and differential thermal analysis curves of BITIVOX gel synthesized by the complex polymerization technique.

Figure 3 shows dilatometric curves of BITIVOX compounds with the following temperature profile: room temperature to 700 °C or 800 °C for a 5 min dwelling and back to room temperature. Figure 3a refers to with and without the application of 200 V cm⁻¹ during 5 min for a programmed 800 °C for 30 min. Figure 3b with the application of 200 V cm⁻¹ during 5 min when the samples reached 700 °C or 800 °C.

The application of the electric field for 5 min when the BITIVOX temperature reached 800 °C Figure 3a) promoted additional 3.2% shrinkage of the sample thickness (13.6–10.4%). The difference may be due to the Joule heating caused by the electric current pulse limited to 1 A through the ceramic pellet. Figure 3b shows the difference in densification when the electric field was applied at two temperatures, 700 °C and 800 °C: the higher the temperature the higher the shrinkage upon applying the same electric field for the same time and electric current limit. A simple explanation is that increasing the temperature decreases the electrical resistivity of the ceramic pellet [$\rho = \rho_0 \exp(H/kT)$, ρ is the resistivity at the absolute temperature T , ρ_0 the pre-exponential factor, H the activation energy and k the Boltzmann constant], allowing for an increase in the electric current J for a constant applied

voltage. The temperature T resulting from the application of the electric field E may be estimated by using the black-body radiation equation $T = [T_0^4 + W/A\sigma]^{1/4}$ [41]. T_0 is the temperature the electric current pulse starts, $A = 1.82 \times 10^{-5} \text{ m}^2$ the pellet parallel surface area, $\sigma = 5.67 \times 10^{-8} \text{ W m}^{-2} \text{ K}^{-4}$ the Stefan-Boltzmann constant, $W = V \times J \times \sqrt{2}/2$ ($V = E \times$ pellet thickness): 2170 °C is the evaluated temperature when the voltage V is applied (time = 0 s in Figure 1) and 1090 °C at 700 °C and 1120 °C at 800 °C at subsequent times, when the power supply voltage drops to keep constant the electric current.

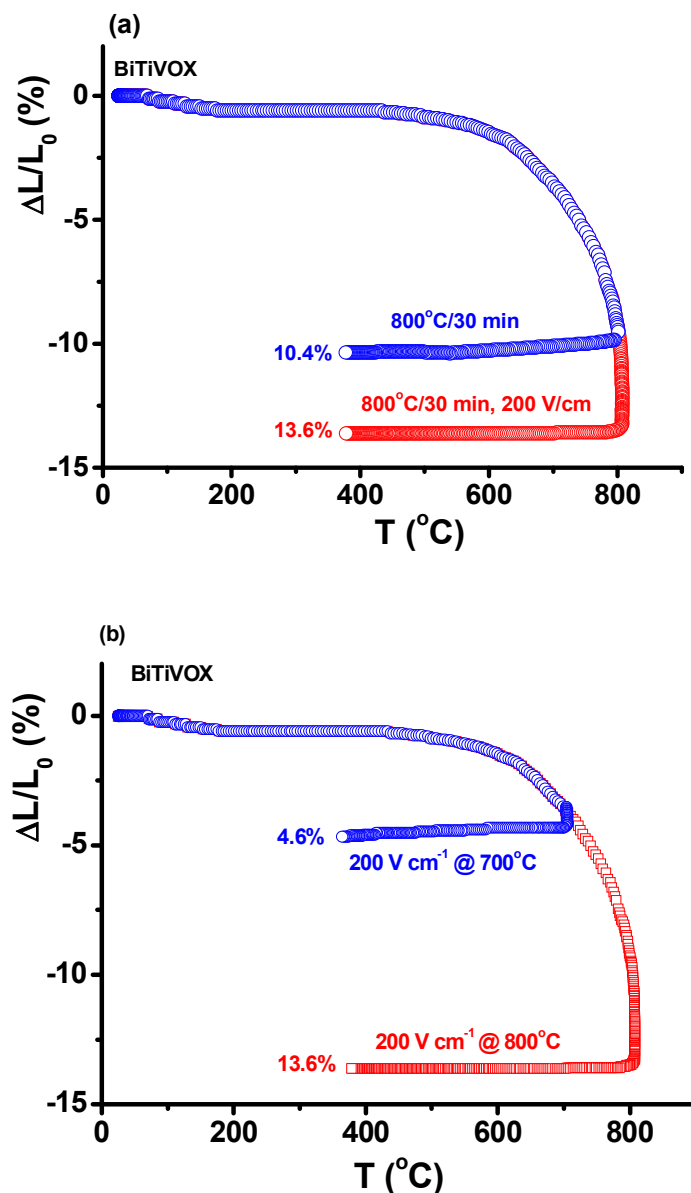


Figure 3. Dilatometric curves of BITIVOX ceramic pellets: (a) heating to 800 °C/30 min without and with application of 200 V cm⁻¹ during 5 min at 800 °C; (b) applying 200 V cm⁻¹ at 700 °C/5 min and at 800 °C/5 min.

Figure 4 shows the results of the impedance spectroscopy measurements at 400 °C of the BITIVOX ceramic pellets sintered according to Figure 3. The BITIVOX sample sintered by applying 200 V cm⁻¹ at 800 °C had bulk electrical resistivity of 0.37 kOhm.cm, while it was 0.76 kOhm.cm without the application of the electric field (Figure 4a). This means that besides the effect of the furnace temperature heating the sample from its outside surface towards the bulk, Joule heating inside the sample due to electric current pulses helps to improve densification. By decreasing the temperature the electric field is

applied, there is an increase in the value of the electrical resistivity (Figure 4b). This result has already been reported for other solid electrolytes and the explanation is simple: higher temperature means lower electrical resistivity and higher amplitude of the electric current, with consequent increased Joule heating, promoting therefore higher densification. An extrapolation to 400 °C of the reported value for the electrical conductivity of the $\text{Bi}_4\text{V}_{1.8}\text{Ti}_{0.2}\text{O}_{11}$ composition sintered at 800 °C for 12 h (electrical conductivity at 320 °C, $\sigma_{320} = 2.56 \times 10^{-5} \text{ S cm}^{-1}$, activation energy $E = 0.61 \text{ eV}$ [32]) leads to $\sigma_{400} = 1.1 \times 10^{-4} \text{ S cm}^{-1}$, which is 25 times lower than the electrical conductivity of our sample flash sintered at 800 °C ($2.7 \times 10^{-3} \text{ S cm}^{-1}$).

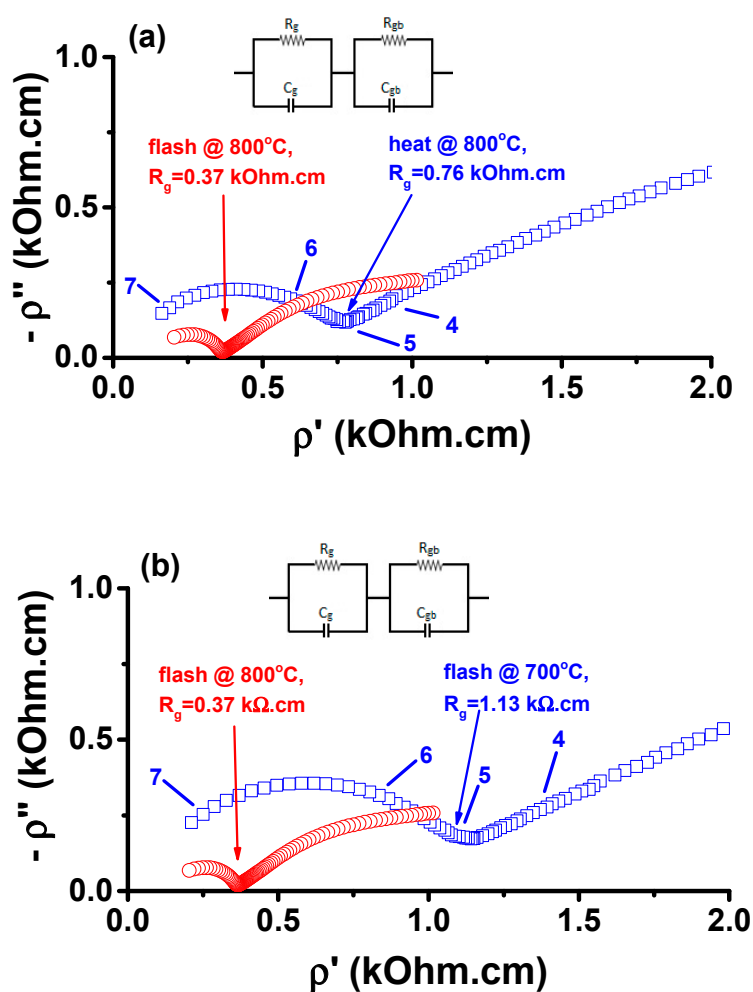


Figure 4. Impedance spectroscopy plots of BITIVOX ceramic pellets and equivalent circuits: (a) sintered at 800 °C/5 min and flash sintered applying 200 V cm^{-1} at 800 °C for 5 min; (b) flash sintered applying 200 V cm^{-1} at 700 °C/5 min and at 800 °C/5 min; Temperature of measurement: 400 °C. Numbers stand for $\log f$ (f : Hz).

Figure 5 shows impedance and Bode diagrams of BITIVOX samples flash sintered at 700 °C and at 800 °C, measured at four temperatures in the 275 °C–400 °C range, for comparison purpose. The diagrams are composed of a skewed semicircle at high frequencies due to the bulk resistivity [42] and a spike at lower frequencies due to electrode polarization [43]. A comparison of the electrical conductivity was possible due to the similar crystallographic phase(s) of all sintered BITIVOX samples (cf. X-ray diffraction results). The sample flash sintered at 800 °C is a better electric conductor (lower electrical resistivity) than the one flash sintered at 700 °C: 4 kOhm.cm (50), 2 (20) kOhm.cm, 0.8 (5.8) kOhm.cm and 0.6 (1.9) kOhm.cm for the flash (conventionally) sintered BITIVOX pellets at 275 °C, 300 °C, 350 °C and 400 °C, respectively.

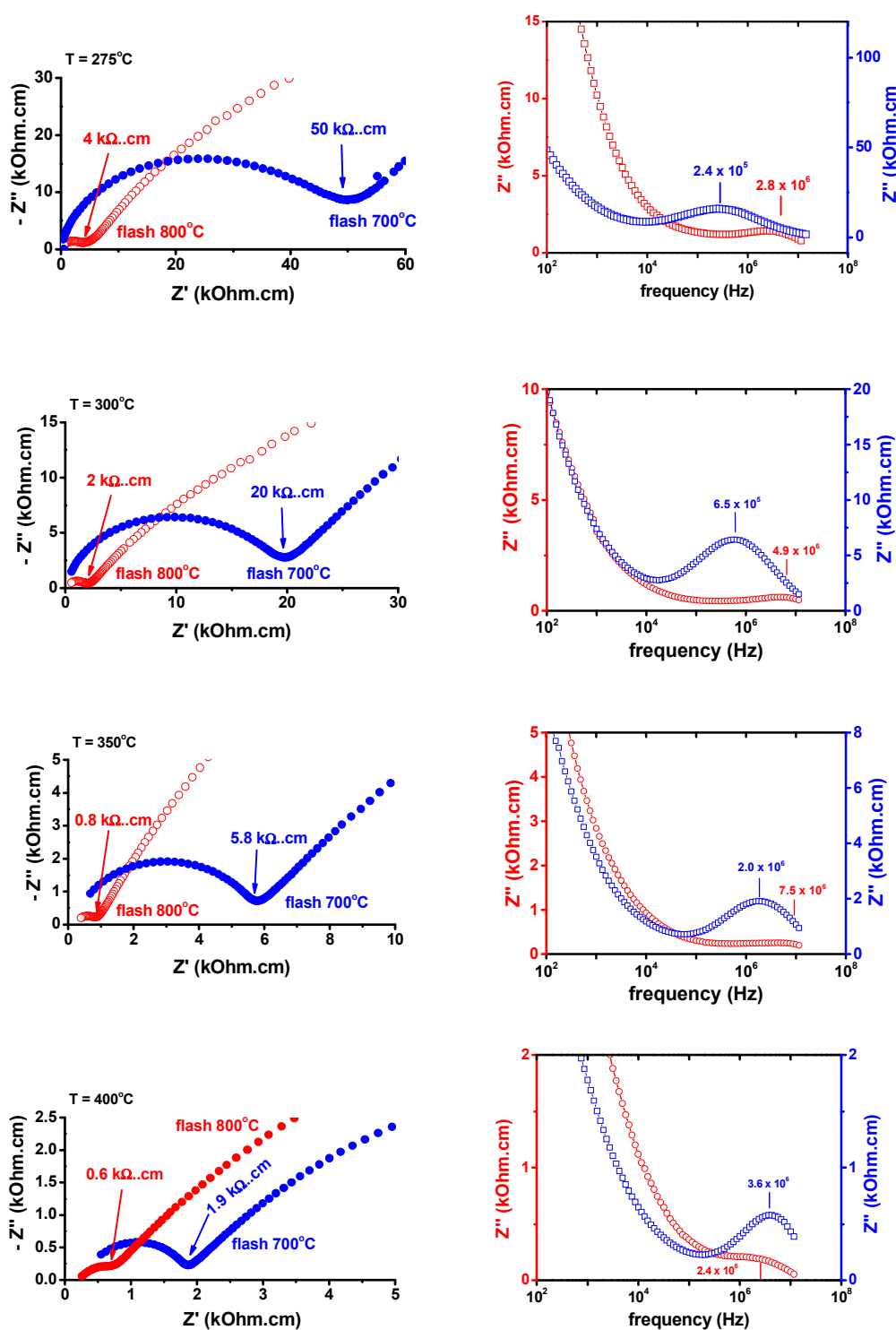


Figure 5. Impedance spectroscopy diagrams (left) and Bode diagrams (right), with data collected at 275 °C, 300 °C, 350 °C, and 400 °C, of BITIVOX samples flash sintered at 700 °C/5 min and at 800 °C/5 min. Bulk resistivity values are shown in the left figures. Maximum frequencies in the right figures.

Figure 6 shows the Arrhenius plots of BITIVOX samples sintered at 800 °C/8 h and flash sintered at 700 °C and 800 °C. The activation energy for the conductive process was determined as 0.78 eV, in agreement with reported values [17,30]. A comparison with reported values for the electrical conductivity and the activation energy is shown in Table 1.

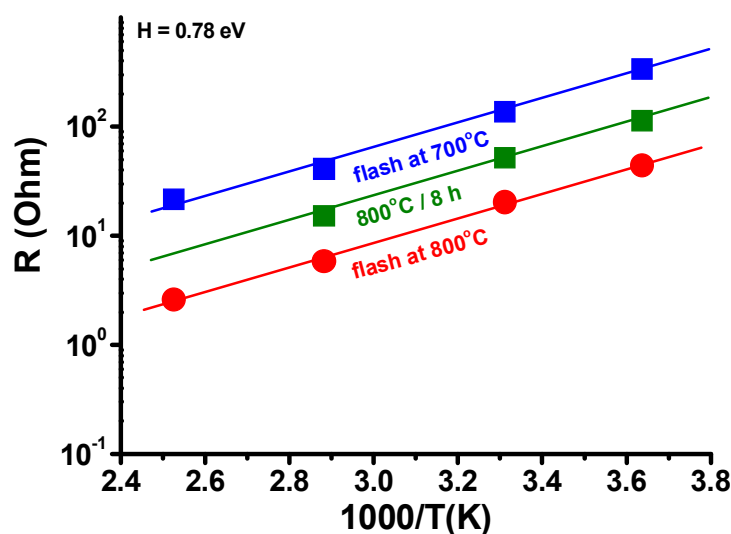


Figure 6. Arrhenius plots of BITIVOX sintered at 800 °C/8 h and flash sintered at 700 °C/5 min and 800 °C/5 min.

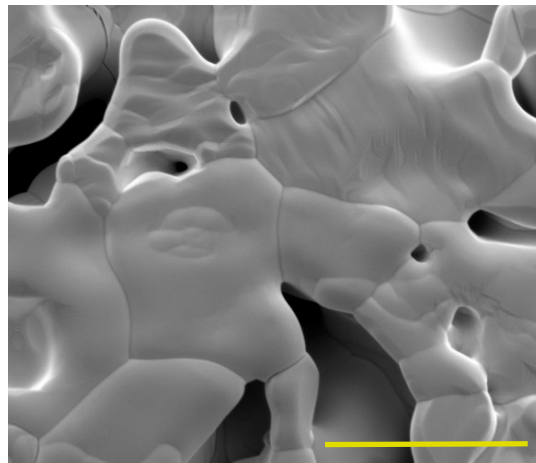
Table 1. Reported and this work values of electrical conductivity σ and activation energy E.

Composition	T (°C)	σ (S cm ⁻¹)	E (eV)	Reference
Bi ₂ V _{0.9} Cu _{0.1} O ₉	227	2.9×10^{-4}	0.66	[44]
Bi ₂ V _{0.9} Ni _{0.1} O ₉	227	3.05×10^{-4}	0.71	[45]
Bi ₂ V _{0.9} Zn _{0.1} O ₉	227	1.27×10^{-4}	0.73	[45]
Bi ₂ V _{0.8} Ti _{0.2} O ₉	320	1.1×10^{-4}	0.61	[32]
Bi ₂ V _{0.8} Ti _{0.2} O ₉	400	3.7×10^{-2}	0.78	this work

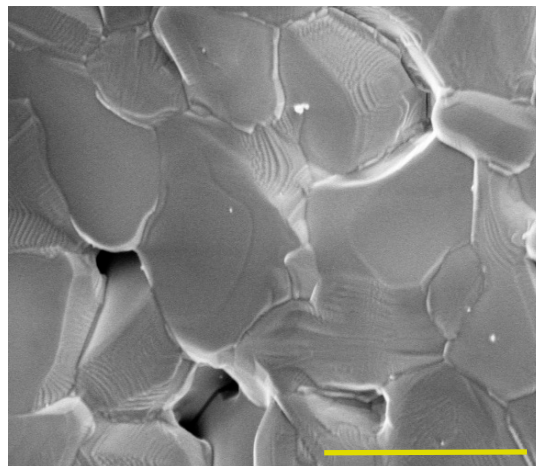
Figure 7 shows the scanning electron microscopy images of surfaces of BITIVOX pellets sintered following different procedures: (a) conventionally in air at 800 °C during 8 h in a resistive furnace; inside a dilatometer by applying 200 V cm⁻¹ at 700 °C (b) and 800 °C (c) during 5 min. The FEG-SEM micrographs indicate a broad distribution of irregular grains of average sizes higher than 1 μ m. The sample flash sintered at 800 °C had larger average grain size than the sample flash sintered at 700 °C, probably due to the lower electrical resistivity, which is exponentially dependent on temperature. The sample flash sintered at 700 °C for 5 min shows grains similar to those of the sample sintered conventionally for 8 h. This means that the electric current was able to produce Joule heating leading to grain growth similar to the sample heated at 800 °C/8 h. The electric current provides also higher mobility of the charge carriers, increasing local Joule heating, promoting grain growth, decreasing porosity, and consequently improving the total conductivity, as shown in Figure 4a.

Intergranular and intragranular pores were observed in the polished surfaces, evidenced by the large contribution to the bulk electrical resistivity (cf. Figure 4).

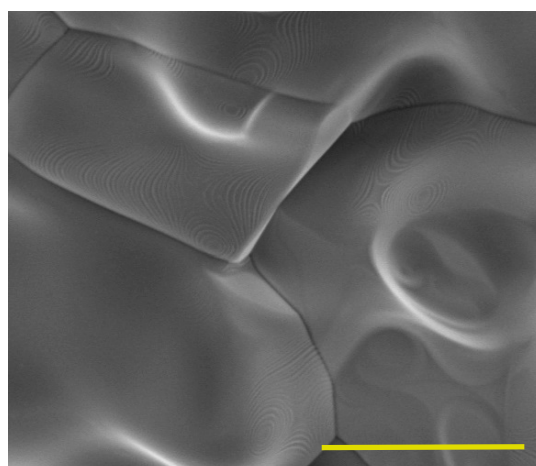
After the scanning electron microscopy and electrochemical impedance measurements, the sintered pellets were ground in an agate mortar for using the powders for the X-ray diffraction analyses. The results are shown in Figure 8. All diffraction patterns are similar with minor residuals of the BiVO₄ parent phase and were indexed for tetragonal the majority phase (PDF 86-0104) [46].



(a) 800 °C/8 h



(b) 200 V cm⁻¹ at 700 °C/5 min



(c) 200 V cm⁻¹ at 800 °C/5 min

Figure 7. Scanning electron microscopy images of BITIVOX solid electrolytes (a) sintered at 800 °C/8 h, (b) sintered with 200 V cm⁻¹ applied at 700 °C/5 min and (c) at 800 °C/5 min. Bar length: 5 μm.

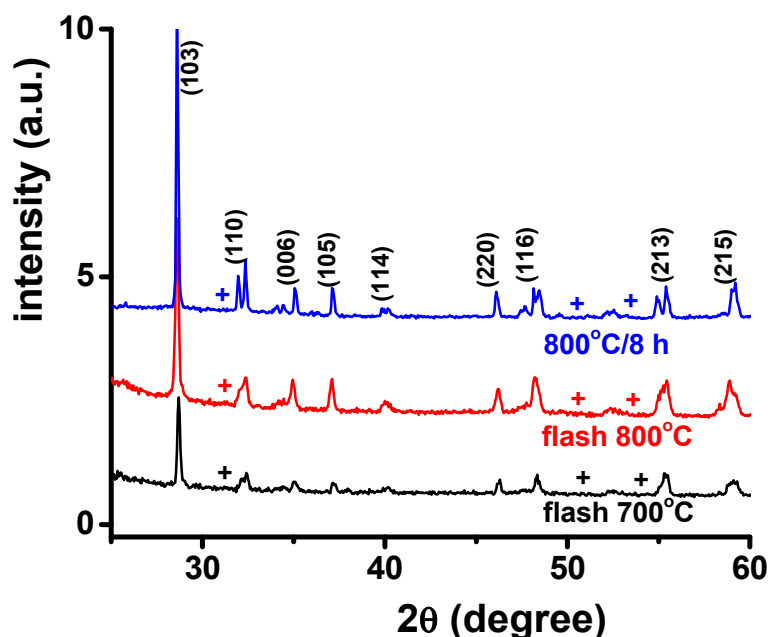


Figure 8. X-ray diffraction patterns of BITIVOX. From top to bottom: sintered at 800 °C/8 h, flash sintered with application of 200 V cm⁻¹ at 800 °C/5 min and at 700 °C/5 min. Also shown the main Miller indices; + location of diffraction peaks of BiVO₄.

4. Conclusions

Bi₄V_{1.8}Ti_{0.2}O₁₁ (BITIVOX) ceramic powders were successfully synthesized by a complex polymerization method followed by calcination at 750 °C. Compacts of the powders sintered by applying AC electric voltages (flash sintering) at 800 °C showed enhanced shrinkage and higher electrical conductivity than compacts flash sintered at 700 °C. Moreover, samples flash sintered at 800 °C for only 5 min achieved larger shrinkage and higher ionic conductivity than samples conventionally sintered by heating at 800 °C for 8 h. Flash sintering is an effective technique for obtaining BITIVOX solid electrolyte pellets in short times with improved electrical conductivity. Further research work is necessary for achieving higher density samples.

Author Contributions: conceptualization, R.M.; methodology, R.M. and E.N.S.M.; formal analysis, R.M., E.N.S.M. and M.S.M.; investigation, M.S.M., S.G.M.C., R.M. and E.N.S.M.; resources, R.M.; writing—original draft preparation, R.M. and M.S.M.; writing—review and editing, R.M., M.S.M., S.G.M.C. and E.N.S.M.; supervision, R.M.; project administration, R.M.; funding acquisition, R.M. and E.N.S.M.

Funding: This research was funded by the Brazilian Agencies: CNEN, CNPq (Procs. 302357/2018-1 and 305889/2018-4) and FAPESP (CEPID-CDMF Proc. 2013/07296-2).

Acknowledgments: R.M. is grateful to Federal University of ABC for the Senior Visiting Researcher fellowship.

Conflicts of Interest: The authors declare no conflict of interest.

References

1. Minh, N.Q. Ceramic Fuel Cells. *J. Am. Ceram. Soc.* **1993**, *76*, 563–588. [[CrossRef](#)]
2. Goodenough, J.B. Oxide-ion electrolytes. *Annu. Rev. Mater. Res.* **2003**, *33*, 91–128. [[CrossRef](#)]
3. Fergus, J.W. Electrolytes for solid oxide fuel cells. *J. Power Sources* **2006**, *162*, 30–40. [[CrossRef](#)]
4. Amado, R.S.; Malta, L.G.B.; Garrido, F.M.S.; Medeiros, M.E. Solid oxide fuel cells: Materials, components and configurations. *Quim. Nova* **2006**, *30*, 189–197. [[CrossRef](#)]
5. Jacobson, A.J. Materials for solid oxide fuel cells. *Chem. Mater.* **2010**, *22*, 660–674. [[CrossRef](#)]
6. Jagannathan, K.P.; Tiku, S.K.; Ray, H.S.; Ghosh, A.; Subbarao, E.C. Technological applications of solid electrolytes. In *Solid Electrolytes and their Application*; Subbarao, E.C., Ed.; Plenum Press: New York, NY, USA, 2012; pp. 201–260.

7. Steele, B.C.H.; Heinzl, A. Materials for fuel cells technology. *Nature* **2001**, *414*, 345–352. [[CrossRef](#)]
8. Overs, A.; Riess, I. Properties of the solid electrolyte gadolinia-doped ceria prepared by thermal decomposition of mixed cerium-gadolinium oxalate. *J. Am. Ceram. Soc.* **1982**, *65*, 606–609. [[CrossRef](#)]
9. Abraham, F.; Boivin, J.C.; Mairesse, G.; Nowogrocki, G. The BIMEVOX series a new family of high performances oxide ion conductors. *Solid State Ion.* **1990**, *40*, 934–937. [[CrossRef](#)]
10. Eguchi, K.; Setogushi, T.; Inoue, T.; Arai, H. Electrical properties of ceria-based oxides and their application to solid oxide fuel cells. *Solid State Ion.* **1992**, *52*, 165–172. [[CrossRef](#)]
11. Huang, P.N.; Petric, A. Superior oxygen ion conductivity of lanthanum gallate doped with strontium and magnesium. *J. Electrochem. Soc.* **1996**, *143*, 1644–1648. [[CrossRef](#)]
12. Lacorre, P.; Goutenoire, F.; Bohnke, O.; Retoux, R.; Lalignant, Y. Designing fast oxide-ion conductors based on $\text{La}_2\text{Mo}_2\text{O}_9$. *Nature* **2000**, *404*, 856–858. [[CrossRef](#)] [[PubMed](#)]
13. Krok, F.; Abrahams, I.; Bangobango, D.G.; Bogusz, W.; Nelstrop, J.A.G. Electrical and structural study of BICOVOX. *Solid State Ion.* **1996**, *86*, 261–266. [[CrossRef](#)]
14. Anne, M.; Bachmann, M.; Pernot, M.; Abrahams, F.; Mairesse, G.; Strobel, P. Structure of new anionic conductors $\text{Bi}_4\text{V}_{2(1-x)}\text{M}_{2x}\text{O}_{11-3x}$, $\text{M}=\text{Cu}, \text{Ni}$. *Physica B* **1992**, *180*, 621–623. [[CrossRef](#)]
15. Sharma, V.; Shukla, A.K.; Gopalakrishnan, J. Effect of aliovalent-cation substitution on the oxygen-ion conductivity of $\text{Bi}_4\text{V}_2\text{O}_{11}$. *Solid State Ion.* **1992**, *58*, 359–362. [[CrossRef](#)]
16. Pernot, E.; Anne, M.; Bachmann, M.; Strobel, P.; Fouletier, J.; Vannier, R.N.; Mairesse, G.; Abraham, F.; Nowogrocki, G. Structure and conductivity of Cu- and Ni-substituted $\text{Bi}_4\text{V}_2\text{O}_5$ compounds. *Solid State Ion.* **1994**, *70*, 259–263. [[CrossRef](#)]
17. Krok, F.; Abrahams, I.; Malys, M.; Bogusz, W.; Nelstrop, J.A.G. Structural and electrical characterisation of BICOVVOX. *Ionics* **1997**, *3*, 235–238. [[CrossRef](#)]
18. Sammers, N.M.; Tompsett, G.A.; Nafe, H.; Aldinger, F. Bismuth based oxide electrolytes structure and ionic conductivity. *J. Eur. Ceram. Soc.* **1999**, *19*, 1801–1826. [[CrossRef](#)]
19. Abrahams, I.; Krok, F.; Malys, M.; Bush, A.J. Defect structure and ionic conductivity as a function of thermal history in BIMGVOX solid electrolytes. *J. Mater. Sci.* **2001**, *36*, 1099–1104. [[CrossRef](#)]
20. Guillodo, M.; Fouletier, J.; Dessemond, L.; Gallo, P.D. Electrical properties of dense Me-doped bismuth vanadate (Me = Cu, Co) p_{O_2} -dependent conductivity determined by impedance spectroscopy. *J. Eur. Ceram. Soc.* **2001**, *21*, 2331–2344. [[CrossRef](#)]
21. Godinho, M.J.; Bueno, P.R.; Orlandi, M.O.; Leite, E.R.; Longo, E. Ionic conductivity of $\text{Bi}_4\text{Ti}_{0.2}\text{V}_{1.8}\text{O}_{10.7}$ polycrystalline ceramics obtained by the polymeric precursor route. *Mater. Lett.* **2003**, *57*, 2540–2544. [[CrossRef](#)]
22. Abrahams, I.; Krok, F. A model for the mechanism of low temperature ionic conduction in divalent-substituted γ -BIMEVOXes. *Solid State Ion.* **2003**, *157*, 139–145. [[CrossRef](#)]
23. Paydar, M.H.; Hadian, A.M.; Fafilek, G. Ionic conductivity and crystal structure relationships in Ti/Cu substituted $\text{Bi}_4\text{V}_2\text{O}_{11}$. *J. Mater. Sci.* **2004**, *39*, 1357–1361. [[CrossRef](#)]
24. Cho, H.S.; Sakai, G.; Shimano, K.; Yamazoe, N. Preparation of BiMeVO_x (Me = Cu, Ti, Zr, Nb, Ta) compounds as solid electrolyte and behavior of their oxygen concentration cells. *Sens. Actuators B* **2005**, *109*, 307–314. [[CrossRef](#)]
25. Chmielowiec, J.; Pasciak, G.; Bujlo, P. Ionic conductivity and thermodynamic stability of La-doped BIMEVOX. *J. Alloys Compd.* **2008**, *451*, 676–678. [[CrossRef](#)]
26. Beg, S.; Salami, N.S. Study on the electrical properties of Co-Ti double substituted $\text{Bi}_4\text{V}_2\text{O}_{11}$. *J. Alloys Compd.* **2014**, *586*, 302–307. [[CrossRef](#)]
27. Beg, S.; Al-Areqi, N.A.S.; Al-Alas, A.; Hafeez, S. Co(III)-Ni(II) double substituted bismuth vanadate: Synthesis, phase stabilization, and structural and electrical characterization. *Ionics* **2014**, *20*, 269–274. [[CrossRef](#)]
28. Fuierer, P.; Maier, M.; Exner, J.; Moos, R. Anisotropy and thermal stability of hot-forged BICUTIVOX oxygen ion conducting ceramics. *J. Eur. Ceram. Soc.* **2014**, *34*, 943–951. [[CrossRef](#)]
29. Roy, V.; Sahu, S.; Avasthi, A.; Bharadwaj, S. Synthesis, electrical and thermal properties of $\text{Bi}_4\text{V}_{2-x}\text{Me}_x\text{O}_{11}$ (Me = Nb, Zr, Y and Cu with $x = 0.0$ and 0.06) ceramics. *J. Therm. Anal. Calorim.* **2014**, *115*, 1265–1271. [[CrossRef](#)]
30. Beg, S.; Haneef, S. Study on phase stability and ionic conductivity in TiIV-substituted bismuth vanadate. *Phase Transit.* **2014**, *87*, 821–831. [[CrossRef](#)]

31. Piva, R.H.; Biz, H.; Piva, D.H.; Morelli, M.R. Facile preparation of BIMEVOX powders via melting process: From synthesis to sintering optimization. *Ceram. Int.* **2016**, *42*, 7088–7098. [[CrossRef](#)]
32. Singh, V.; Gosh, S.; Aich, S.; Roy, B. Low temperature solid oxide electrolytes (LT-SOE): A review. *J. Power Sources* **2017**, *339*, 103–135. [[CrossRef](#)]
33. Yang, D.; Conrad, H. Enhanced sintering rate of zirconia (3Y-TZP) by application of a small AC electric field. *Scr. Mater.* **2010**, *63*, 328–331. [[CrossRef](#)]
34. Muccillo, R.; Kleitz, M.; Muccillo, E.N.S. Flash grain welding in yttria stabilized zirconia. *J. Eur. Ceram. Soc.* **2011**, *31*, 1517–1521. [[CrossRef](#)]
35. Grasso, S.; Sakka, Y.; Rendtorff, N.; Hu, C.; Maizza, G.; Borodianska, H.; Vasykiv, O. Modeling of the temperature distribution of flash sintered zirconia. *J. Ceram. Soc. Japan* **2011**, *119*, 144–146. [[CrossRef](#)]
36. Raj, R. Joule heating during flash sintering. *J. Eur. Ceram. Soc.* **2012**, *32*, 2293–2301. [[CrossRef](#)]
37. Dancer, C.E.J. Flash sintering of ceramic materials. *Res. Express* **2016**, *3*, 102001. [[CrossRef](#)]
38. Yu, M.; Grasso, S.; McKinnon, R.; Saunders, T.; Reece, M.J. Review of flash sintering: Materials, mechanisms and modelling. *Adv. Appl. Ceram.* **2016**, *116*, 24–60. [[CrossRef](#)]
39. Muccillo, R.; Muccillo, E.N.S. An experimental setup for shrinkage evaluation during electric field-assisted flash sintering: Application to yttria-stabilized zirconia. *J. Eur. Ceram. Soc.* **2013**, *33*, 515–520. [[CrossRef](#)]
40. Kleitz, M.; Kennedy, J.H. Resolution of multicomponent impedance diagrams. In *Fast Ion Transport in Solids*; Mundy, J.N., Shenoy, G.K., Vashishta, P., Eds.; Elsevier North Holland, Inc.: New York, NY, USA, 1979; pp. 185–188. ISBN 0444003533.
41. Muccillo, E.N.S.; Muccillo, R. Electric field-assisted sintering of tin dioxide with manganese dioxide addition. *J. Eur. Ceram. Soc.* **2014**, *34*, 3699–3706. [[CrossRef](#)]
42. Fletcher, J.G.; West, A.R.; Irvine, J.T.S. The AC-impedance response of the physical interface between yttria-stabilized zirconia and $\text{YBa}_2\text{Cu}_3\text{O}_{7-x}$. *J. Electrochem. Soc.* **1995**, *142*, 2650–2654. [[CrossRef](#)]
43. Barsoukov, E.; Macdonald, J.R. *Impedance Spectroscopy: Theory, Experiment, and Applications*, 2nd ed.; John Wiley and Sons, Inc.: Hoboken, NJ, USA, 2005; ISBN 978-0471647492.
44. Dygas, J.R.; Krok, F.; Bogusz, P.; Kurek, P.; Reiselhuber, K.; Breiter, M.W. Impedance study of BICUVOX ceramics. *Solid State Ion.* **1994**, *70–71*, 239–247. [[CrossRef](#)]
45. Kurek, P.; Breiter, M.W. Thermal stability and ionic conductivity of the BIMEVOX.10 ceramics (ME = Zn, Ni). *Solid State Ion.* **1996**, *86–88*, 131–135. [[CrossRef](#)]
46. Tripathy, D.; Pandey, A. Structural and impedance studies of TiIV and NbV co-doped bismuth vanadate system. *J. Alloys Compd.* **2018**, *737*, 136–143. [[CrossRef](#)]



© 2019 by the authors. Licensee MDPI, Basel, Switzerland. This article is an open access article distributed under the terms and conditions of the Creative Commons Attribution (CC BY) license (<http://creativecommons.org/licenses/by/4.0/>).